In-vivo Effects of Different Orthodontic Loading on Root Resorption and Correlation to Mechanobiological Stimulus in Periodontal Ligament

Jingxiao Zhong[1], Junning Chen[2,3], Richard Weinkamer[3], M. Ali Darendeliler[4], Michael V. Swain[1,4], Andrian Sue[1], Keke Zheng[1], Qing Li[1]

[1]School of Aerospace, Mechanical and Mechatronic Engineering, University of Sydney, Australia

[2]College of Engineering, Mathematics and Physical Sciences, University of Exeter, U.K.

[3]Department of Biomaterials, Max Planck Institute of Colloids and Interfaces, Germany

[4]Faculty of Dentistry, Discipline of Orthodontics, University of Sydney, Australia

Short Title: Orthodontic Root Resorption and Mechanobiology

*Corresponding Author: Qing Li

Address: The University of Sydney, NSW 2006, Australia

Phone: +61-2-9351-8607

Fax: +61-2-9351-7060

E-mail: qing.li@sydney.edu.au

Abstract

Orthodontic root resorption (ORR) is a common side effect of orthodontic therapy. It has been known that high hydrostatic pressure in the periodontal ligament (PDL) generated by orthodontic forces will trigger recruitment of odontoclasts, leaving resorption craters on root surfaces. The patterns of resorption craters are the traces of odontoclast activity. This study aimed to investigate resorptive patterns by: (1) quantifying spatial root resorption under two different levels of *in-vivo* orthodontic loadings using microCT imaging techniques; and (2) correlating the spatial distribution pattern of resorption craters with the induced mechanobiological stimulus field in PDL through nonlinear finite element analysis (FEA) *in silico.*

Results indicated that the heavy force led to a larger total resorption volume than the light force, mainly by presenting greater individual crater volumes ($p < 0.001$) than increasing crater numbers, suggesting that increased mechano-stimulus predominantly boosted cellular resorption activity rather than recruiting more odontoclasts. Furthermore, buccal-cervical and lingual-apical regions in both groups were found to have significantly larger resorption volumes than other regions ($p < 0.005$). These clinical observations are complimented by the FEA results, suggesting that root resorption was more likely to occur when the volume average compressive hydrostatic pressure exceeded the capillary blood pressure (4.7kPa).

Keywords: orthodontic root resorption, nonlinear finite element analysis, mechano-stimulus, periodontal ligament, odontoclastic activity

1. Introduction

Orthodontic treatment is widely applied in dental practice to align teeth into more functionally and aesthetically favourable positions[1]. Apart with its proven benefits, orthodontic root resorption (ORR) is one of the major adverse effects of orthodontic treatment, which is the abnormal breakdown of tooth structure, leaving root surfaces with resorption craters [2-4]. Unlike physiological root resorption, ORR signifies a complex mechanobiological process, which may involve hyalinization, inflammation, and demineralization of the cementum and dentin under certain conditions generated by orthodontic forces [5]. Once ORR reaches the dentin layer, destruction of root surfaces are generally considered irreversible [6], and it potentially leads to the premature loss of the affected teeth if untreated [7, 8].

In spite of considerable progress in understanding cellular activity associated with bone remodelling during orthodontic tooth movement (OTM), ORR remains understudied in terms of cellular response to mechanical stimulus. While its mechanobiology has not been fully understood, ORR remains an undesired but unavoidable iatrogenic consequence of orthodontic treatment; and its severity and potential damage is difficult to predict [9]. Some studies have suggested that, similar to bone remodelling around a tooth [10, 11], ORR is a response mediated by the compressed periodontal ligament (PDL) [12-14], whereby the hydrostatic pressure of the interstitial fluid in the PDL tissue limits nutrition delivery and generates the mechanobiological signals to recruit monocytes and macrophages from vascular spaces, giving rise to cell mitosis and differentiation [15]. This biological process further leads to the differentiation of macrophages into odontoclasts to resorb the mineralised root surfaces [12, 13, 16, 17].

Odontoclasts are the main cell type responsible for ORR. Animal studies showed that root

resorption occurred in the areas where invading odontoclasts were observed [17, 18]. Odontoclasts are multi-nucleated giant cells that originate from hematopoietic stem cells, and are the descendants of the monocyte and macrophage cell lineage [19]. Apart from being smaller in size and having fewer nuclei, odontoclasts were suggested to be highly similar to osteoclasts in several reports [18-20], not just along the differentiation pathway but also in their desired function of resorbing mineralised tissue. It has been demonstrated that odontoclasts and osteoclasts share a common mechanism in the cellular resorption of dental hard tissue [18]. While osteoclasts have been extensively studied for their responses to mechano-stimuli [21-25], few reports have investigated the behaviours of odontoclasts [18, 26].

In orthodontic practice, the treatment-related risk factors are of particular interest to clinicians [9], and orthodontic load magnitude is believed to be one of the primary controlling factors, which is amenable to regulate treatment outcome. A proper level of load could lead to the maximum amount of tooth movement with minimum resorption [27, 28]. Intricate anatomical and physiological environment for ORR makes *in-vivo* investigation infeasible, therefore, most studies on osteoclasts/odontoclasts were *in-vitro* [18, 19], and their responses to mechanobiological loading have yet to be studied.

To further understand the mechanobiology behind ORR, it is essential to investigate the links between orthodontic loading, mechanobiological stimulus and odontoclastic activity. For such a 3-dimensional (3D) phenomenon, micro computed tomography (microCT) provides the current gold standard to quantify ORR volumetrically [27, 29, 30], though the spatial patterns of its extent and distribution have not yet been critically investigated, in particular its association with orthodontic loading. Clinically, there are limited approaches available for evaluation of mechanobiological

stimulation induced by a given mechanical loading. Finite element (FE) methods have on the other hand exhibited compelling advantages in biomechanical analysis, with sophisticated anatomical models and nonlinear soft-tissue responses [11, 31]. Therefore, in this study, 3D subject-specific FE models were created based on the microCT images to evaluate the corresponding mechanobiological stimuli induced by different orthodontic loadings.

This study aimed to investigate the mechanobiological relationship between crater formation in ORR and clinically applied orthodontic loading. Since direct monitoring of cellular activities in human subjects remain infeasible, this work combines *ex-vivo* experimental and *in-silico* numerical methods, providing an alternative approach to understanding the correlation between ORR and orthodontic loading. In doing so, this work develop an effective step towards predictive modelling for therapeutical prognosis, potentially improving treatment outcome in such a sophisticated orthodontic procedure.

2. Methods

2.1. Clinical Treatment and Sample Preparation

Ethics approval was obtained from the Human Research Ethics Committee at the University of Sydney (Number 8782). 10 patients (7 female and 3 male), whose 1st premolars were required to be extracted as a part of their orthodontic treatment plans, were recruited for this study, with a mean age of 14.3 ± 1.9 years old. These participants were selected based upon the same criteria as in the previous studies, of which the most important is an absence of abnormalities and defects existing on roots prior to the orthodontic treatment [27]. All the subjects and their guardians consented to the participation after receiving verbal and written explanations of all aspects of this study, including the outcomes of tooth movement, and potential discomforts. A panoramic radiograph and lateral

cephalogram were taken for each patient, as an initial check prior to orthodontic treatment to ensure no abnormalities or defects were present in the targeted teeth (Figure 1a).

The mandibular 1st premolars (tooth numbers #34 and #44) in the subjects were the target teeth in this study. To reduce inter-individual variability in each of these ten investigated patients, the left and right first premolars were randomly selected for receiving the two different levels of orthodontic loads, namely light (25 g, i.e 0.245 N) and heavy (225 g, i.e 2.2 N) forces (Figure 1b), which are the typical upper and lower limits of orthodontic loadings applied clinically [27, 29, 32]. 0.022-in Speed brackets (Strite Industries, Cambridge, Ontario, Canada) were bonded to the mandibular 1st premolar and 1st permanent molar, to induce a tipping load in the buccal direction (labelled in Figure 1b) of the premolar. The light force was generated by using a 0.016-in titanium-molybdenum alloy (TMA, Rematitan, Dentaurum, Ispringen, Germany) cantilever spring; and the heavy force was from a 0.025-in TMA cantilever spring (beta III titanium, 3M Unitek, Monrovia, Calif). These orthodontic loads were calibrated and adjusted to the desired force magnitude with a strain gauge (Dentaurum, Ispringen, Germany) every four weeks [27, 33]. Light cured cement (Transbond Plus light cure band adhesive, 3 M Unitek) was placed on top of 1st molars, to create a gap between the targeted 1st premolars and maxillary premolars, and, therefore, avoiding undesired effects from occlusal loading (Figure 1b).

After 12 weeks of loading, the treated premolars were extracted carefully to prevent surgical trauma to the root cementum and immediately stored separately in sterilized deionized water (Milli Q, Millipore, Bedford, Germany). The residual PDL and soft tissue fragments were removed by placing each tooth in an ultrasonic bath for 10 minutes. The teeth were then kept in 70% alcohol for 30 minutes and dried at ambient room temperature.

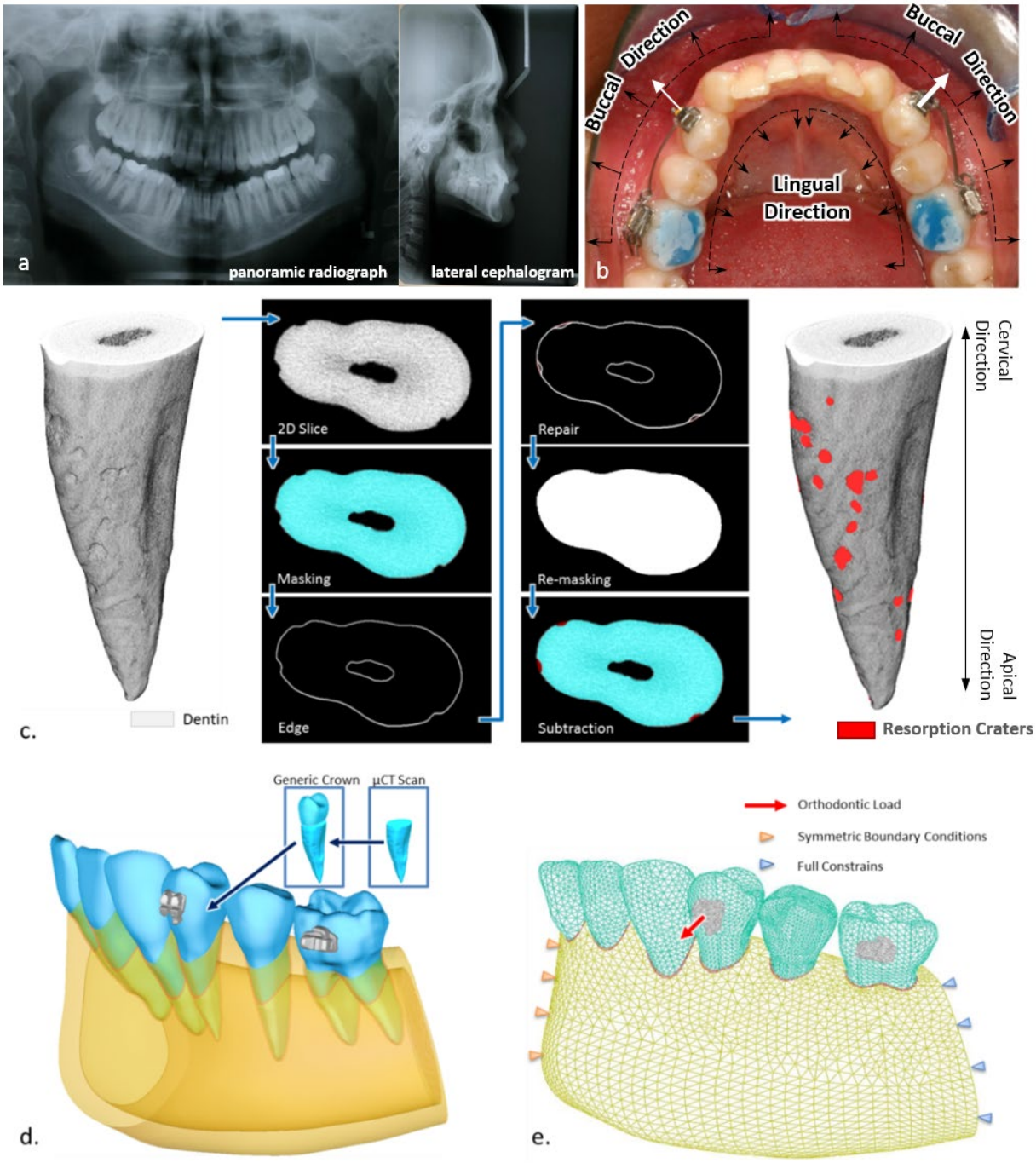

Figure 1. Materials and Methods. a) An initial panoramic radiograph and lateral cephalogram were taken for each patient to ensure no abnormalities and resorption defects were present before treatment. b) Top view of orthodontic treatment setup including braces between the mandibular 1st molar and the 1st premolar and cement on top of the 1st molars (bluish). White arrows indicate buccally-directed orthodontic loads. Black arrows indicate the buccal and lingual directions, i.e. the outwards direction to the cheek and inwards direction to the tongue. c) schematic diagram of the Tomographic Interpolation and Volumetric Analysis (TIVA) procedure to determine resorption craters from a scanned root, through masking tooth root (cyan), edging (white), contour repair (white: original edge; red: repaired edge), re-masking (white), and mask subtraction (cyan: original tooth root mask; red: resorption craters mask). Black arrows indicate the orientation of the tooth with cervical defined towards the crown and apical towards the root apex. d) construction of a virtual assembly of the mandibular section by using virtually repaired root contour; e) meshed finite element model in commercial code ABAQUS with loading and boundary conditions.

2.2. Imaging, Segmentation and Tomographic Quantification

The prepared samples were scanned from the cementoenamel junction towards the root apex using a microCT scanner SkyScan 1172 (SkyScan, Aartselaar, Belgium) with an aluminium filter. Some samples were able to be included into one field of view, while the others were merged from two sectional scans along the root longitudinal axis. The scans were performed under 100 kV and 100 μA, and each scan took 44 minutes. The reconstructed scans had a linear pixel size between 14.8 and 15.9 μm and were saved in a 16-bit TIFF format. The image sets were imported into ScanIP Ver. 7.0 (Simpleware, Exeter, United Kingdom) for segmentation, creating tooth root masks based upon greyscale values and exported for further analysis.

In our previous studies, the pre-existing volume of craters were quantified on non-treated teeth with an average of 4.21 × 105 um3, in comparison with the average of 291.69 × 105 um3 in the treated teeth with a light orthodontic force (less than 1.5%) [29, 32]. Since the same subject selection criteria and treatment procedure were used in the current study, the crater volume before the treatment can be therefore considered as negligible. For doing so, a MATLAB (MathWorks Inc., Natick, MA, United States) program was developed specifically for the present study, namely Tomographic Interpolation and Volumetric Analysis (TIVA), a virtual computational 'repair' tool for reinstating the tangential continuity of the root surface by using Gaussian smoothing algorithm, while the unaffected regions remained unchanged. In this way, the intact root was virtually restored to estimate the pre-treatment condition on the assumption that non-treated root surfaces of the selected healthy and young participants were smooth with negligible pre-existed site-defects.

Image subtraction of the virtually restored root and the post-treatment root yields the 3D resorption crater. As some craters were very close or even connected with each other, the virtual CT

slices of resorption craters were imported into ScanIP Ver. 7.0 for watershed segmentation (Simpleware, Exeter, United Kingdom) to separate connected craters by defining their individual boundaries. For each crater, TIVA then quantified its geometric characteristics including pixel-based volume (individual crater size), centroid location, maximum depth, surface long (Ax) and short axes (Bx), and orientations (angle between the surface long axes and root longitudinal axis). The statistics for all the data were then analysed and performed in IBM SPSS Ver. 19 (IBM Corp., Armonk, NY, United States) for paired t-tests.

2.3. Finite Element Modelling and Simulation

The hydrostatic stress within PDL is quantified at a steady state prior to bone remodelling and ORR initiation. Volume averaged hydrostatic stress ($\bar{\sigma}_H$) in the PDL has been widely adopted to be the mechano-stimulus for governing dental mineral tissue remodelling [11, 31]. The present study utilised 3D nonlinear finite element analysis (FEA) technique to obtain $\bar{\sigma}_H$ in the PDL that was induced by orthodontic force during the treatment, calculated as $\bar{\sigma}_H = \frac{\sum_e \sigma_H^e V^e}{\sum_e V^e}$, where the σ_H^e is the hydrostatic stress within each element and V^e is the volume at the integral point of corresponding element. The values of $\bar{\sigma}_H$ will be used to divulge a possible correlation between the root resorption and mechano-stimulus.

All the numerically repaired root masks were exported in a format of STL files and processed in Geomagic Wrap 2015 (3D Systems, Rock Hill, United States). The scanned premolar was virtually inserted into a generic mandible model (Figure 1d), in which the neighbouring teeth were arranged according to the condition of an individual patient, thereby providing a simulated oral environment corresponding to the clinical cases.

The periodontal ligament (PDL), as a critical biomechanical medium for governing orthodontic

tooth movement and ORR, was created by smoothly offsetting the root outer surface by 0.3 mm, which was the average thickness of human PDL [11, 15, 31]. The dedicated FE sensitivity tests, with both constant and varying thickness PDL models, were conducted to quantify the robustness of the obtained results. The numerical results showed that the volume fraction of PDL that exceeded capillary blood pressure hovered around 89.4% ± 2.1% when the thickness was ranged between 0.1 and 0.5 mm.

The brackets for attachments were constructed in computer-aided design (CAD) software, Solidworks Ver. 2016 (Dassault Systèmes, Waltham, United States), and inserted at the corresponding locations in the assembly. The assemblies were constructed into a solid model by using non-uniform rational B-spline (NURBS) patches and imported into ABAQUS Ver. 6.14.1 (Dassault Systèmes, Waltham, United States) for meshing and analysis (Figure 1e).

Unstructured quadratic tetrahedral elements (C3D10H) were used to smoothly capture anatomical details with an adaptive mesh in a global seed size of 1 mm, while particularly intensified mesh-refinement was applied to all PDL regions. The average number of elements was 204,369 (with a degree of freedom (DOF) of 888,990), of which around 17,575 (with a DOF of 97,323) were dedicated to the PDLs (with an average individual volume of ~ 46.3 mm^3). The mesh density was validated through a convergence test as done in our previous studies [11, 31].

Since the effects from occlusal loading were eliminated and the simulation focussed only on the initial stage of the orthodontic treatment, the PDL was considered to be in a quasi-static status with a stabilised fluid phase. Therefore, a nonlinear hyperelastic mathematical constitutive model was adopted for the PDL here by fitting the stress-strain curve [34] to the 4th Order Ogden Model as presented in ABAQUS [11]. The 4th order Ogden model is a strain energy potential equation that can

be expressed as: $U = \sum_{i=1}^{4} \frac{2\mu_i}{\alpha_i^2}\left(\bar{\lambda}_1^{\alpha_i} + \bar{\lambda}_2^{\alpha_i}\bar{\lambda}_3^{\alpha_i} - 3\right) + \sum_{i=1}^{4} \frac{1}{D_i}(J^{\varepsilon I} - 1)^{2i}$, in which $\bar{\lambda}_i$ are the deviatoric principal stretches obtained from the principal stretches, $J^{\varepsilon I}$ is the elastic volume strain, and μ_i, α_i and D_i are the parameters used in such a hyperelastic model [35]. The hyperelastic constitutive model was also proposed to fit PDL's viscoelastic behaviour [34], and has been adopted widely in dental biomechanics [11, 36]. Its accuracy had also been validated [34] by correlating with the previous *in-vitro* studies on PDLs of human cadavers [37] as well as other mathematical models [37, 38].

Linear elastic and isotropic properties (Table 1) [11, 31, 39, 40] were assigned to the remaining regions in the model, including the cancellous and cortical regions of the two-phase jaw model and the dentition regions. The assumption of such two-phase jaw model was tested by comparing the outcome with the results from a patient-specific heterogeneous jaw model [41, 42]. The difference in the variation of the volume fraction of the PDL that exceeded capillary blood pressure was smaller than 0.1%.

Table 1. Material properties adopted in tooth movement simulation

Material	Young′s Modulus (MPa)	Poisson′s Ratio
Root (Dentin)	18,600	0.31
Cortical bone	14,700	0.31
Trabecular bone	490	0.3
PDL	Hyperelastic (Ogden 4th)	0.45

Symmetric boundary conditions were prescribed to the sagittal plane of the mandibular section, and full constraints were applied to the distal sectional planes (Figure 1e). The orthodontic forces were applied through the premolar bracket, pointing in the buccal direction [11]. Friction and slipping between the brackets and the arch wire were not considered in this study for simplification [11, 12].

3. Results

3.1. Resorption Severity Overview

Figure 2a presents the orthodontic root resorption (ORR) patterns from both buccal and lingual aspect views of the target premolars, under the two levels of orthodontic forces (25g and 225g) used for each subject. An initial visual inspection suggests that on the buccal side, more craters were formed in the cervical region (labelled in Figure 1c); while on the lingual side they had a tendency to crowd around the apical regions (labelled in Figure 1c). In the apex areas, craters tended to develop along the peri-groove regions while the roots with deep and clear grooves seemed to have more craters than those without such features. Figure 2b summarises the distance of OTM in the lingual-buccal direction from clinical measurement. Unfortunately, OTM for patient 8 and 9 were not recorded properly because of human errors.

To quantitatively assess the resorption, Figure 2c summarises the total resorption volume and the total number of craters in each patient. In general, the heavy orthodontic force led to more severe resorption than the light force in terms of both volume (Light: 0.16 ± 0.16 mm^3 vs. Heavy: 0.59 ± 0.31 mm^3, $\rho < 0.001$) and number of craters (Light: 24.8 ± 11.1 vs. Heavy: 37.9 ± 17.6, $\rho < 0.05$). Resorption severity varied among the subjects. It is noted that for example patient 8 had minimal resorption volumes, while patient 5 had substantially more severe resorption on both light and heavy loaded teeth than the other subjects. Besides, an individual's response to two different levels of force varied dramatically among the subjects. In terms of resorption volume, the most significant differences appeared in Patients 10 and 6, in which the heavy force led to 15.6 and 10.8 times of the resorption than that of the light force, respectively. Patient 8 had the least difference with only 1.24 times. Interestingly, the number of craters is not necessarily proportional to the total volume of

resorption. Patients 3 and 4 had fewer numbers of craters under the heavy force; and Patient 8 had roughly the same number at both force levels.

Figure 2d indicates the distribution of crater sizes. Similarly to the total volume, the heavy force caused both larger maximum craters ($\rho < 0.001$) and larger median size craters ($\rho < 0.005$) than the light force in all subjects.

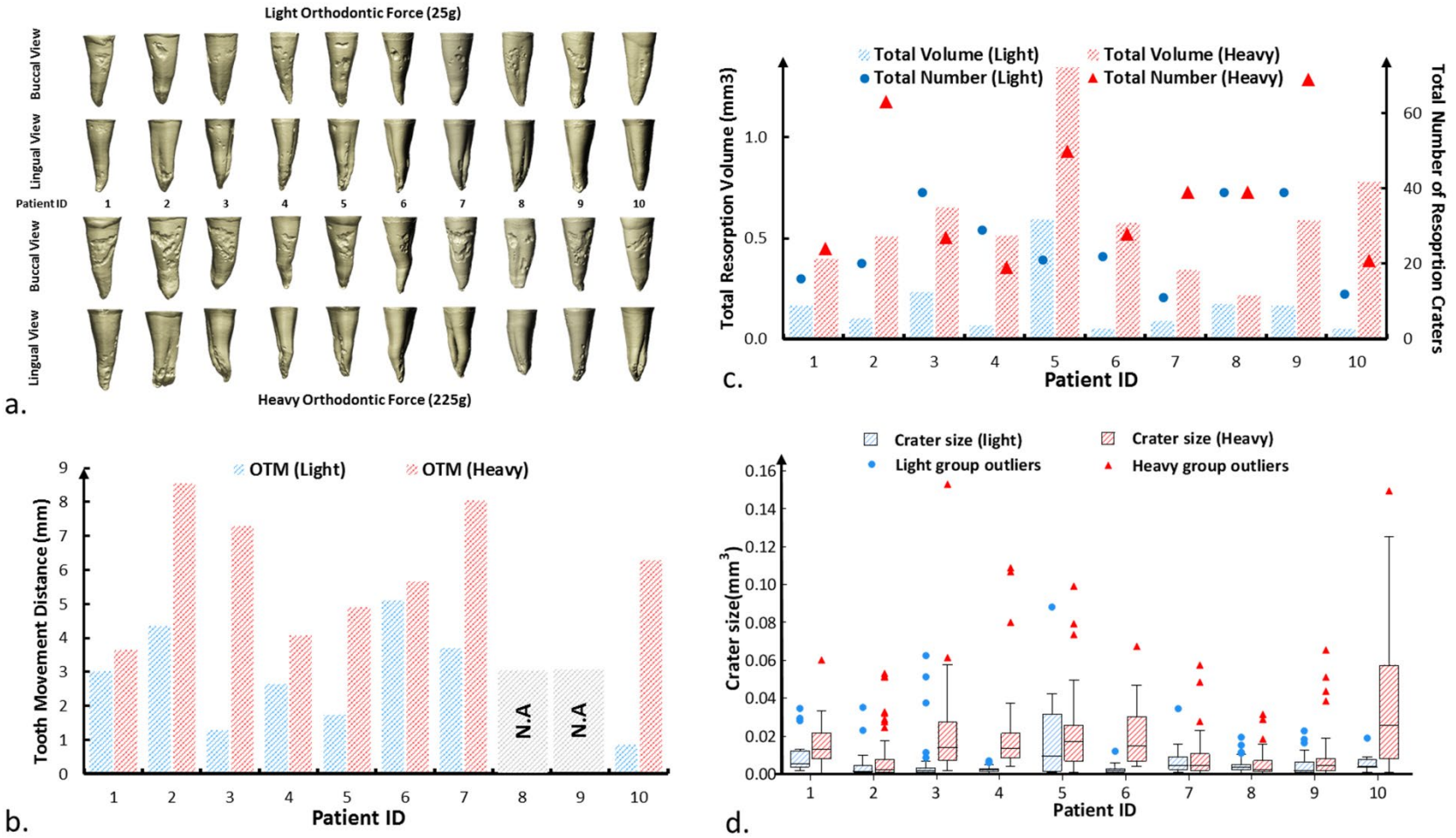

Figure 2. Resorption Severity. a) Surface tomography of ten pairs of scanned 1st premolar roots, between heavy (225g) and light (25g) buccally directed orthodontic forces; b) Clinical records of Orthodontic Tooth Movement (OTM) among patients. c) total resorption volume and number of resorption craters for each patient; d) crater sizes in each patient. The Heavy group generally had larger craters than the Light group did. (The upper and lower box bands are the 1st and 3rd quartile, representing 25% to 75% of size observations. The bands inside boxes represent the median crater size for each subject. Craters with a size that exceeded 1.5 times that of the corresponding interquartile range are plotted as outliers in this box-whisker chart.)

3.2. Individual Crater Characteristics

Figure 3 illustrates the characteristics of individual craters. The length of the long axis (Ax) at the crater surface was used to evaluate their surface size. Figures 3a and 3b clearly indicate that the length and depth of craters had a linear relationship for both groups, which had similar average slopes with 0.094 for the light and 0.092 for the heavy group, implying that the ratio between surface size and resorption depth was not much affected by the orthodontic loading magnitude.

Figures 3c and 3d exhibit the spatial orientation of individual craters. Craters were more prone to orient along the longitudinal direction of the root in a range of 0° to 45° in both groups. This holds, particularly, for elongated craters with a surface long axis to short axis ratio (i.e. Ax/Bx) > 2 (Figures 3c and 3d). Similarly to the relationship between depth and surface size, this individual orientation pattern was marginally influenced by loading magnitude.

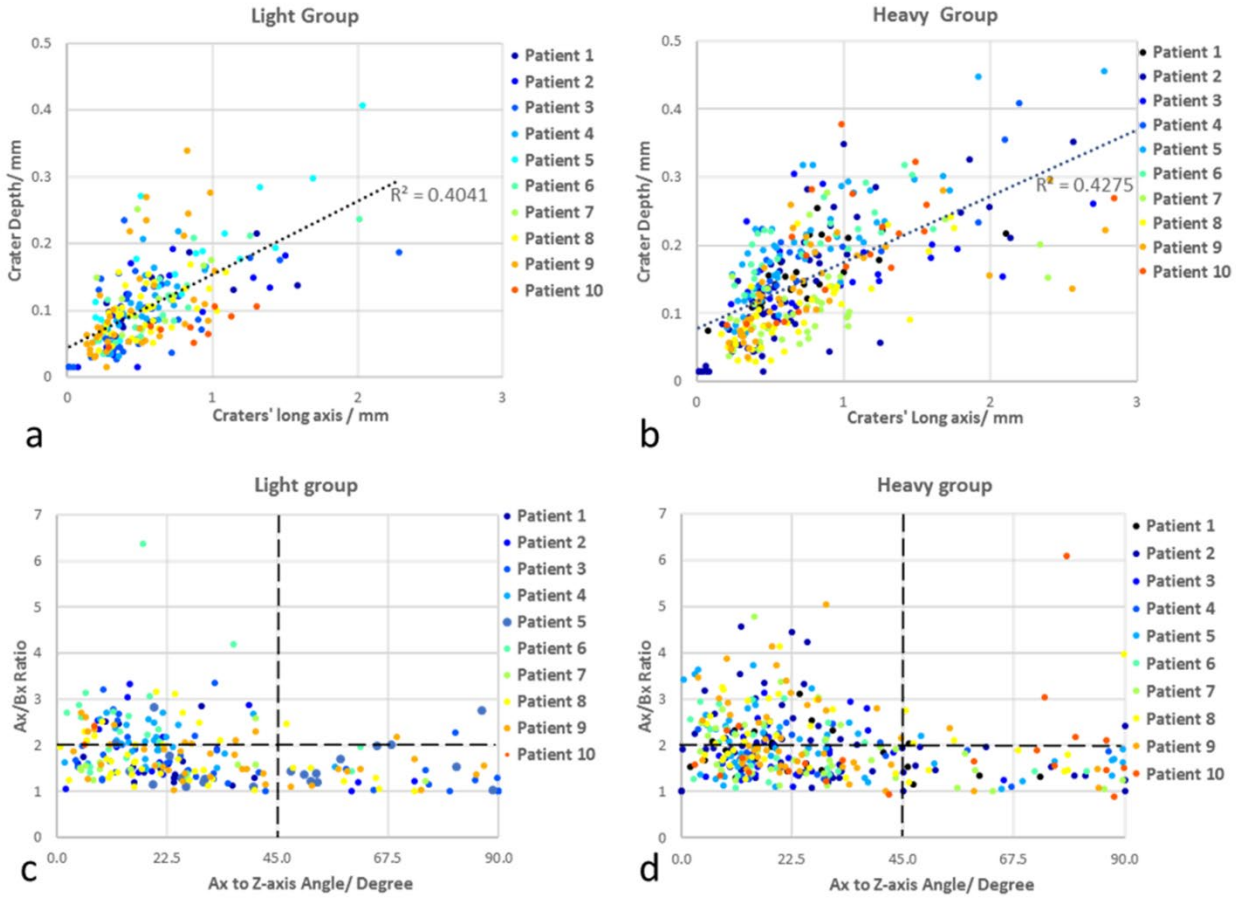

Figure 3. Crater Characteristics. a) and b) Correlation between resorption crater surface area and depth under light and heavy forces; c) and d) Correlation between crater orientation and surface aspect ratio, under light and heavy forces. Ax represents the surface long axis of craters whereas Bx represents the surface short axis. Z-axis is the longitudinal axis of the root.

3.3. Spatial Location of Resorption Craters

For a spatial analysis of resorption patterns, each root was divided into four sectors: lingual, buccal, distal, and mesial regions (Figure 4a). Regional resorption volume of an individual patient is summarised in Figures 4c and 4d for the light and heavy force groups, respectively. In the light force group, most resorption appeared in the lingual and buccal regions for all the subjects except for Patient 2 who had considerable resorption in the mesial aspect. In the heavy force group, this pattern was further emphasised, and all the subjects exhibited dominant resorption in the lingual-buccal direction, along the loading axis.

As the lingual and buccal sectors appeared to be more prone to resorption, Figure 4b further separates the root into four sectors along the long axis of the root, namely the cervical-buccal, apical-buccal, cervical-lingual, and apical-lingual sectors. Figures 4e and 4f illustrate that most resorption occurred in the cervical-buccal sector in every subject ($\rho < 0.005$); and the apical-lingual sector had the second most severe resorption ($\rho < 0.005$). It is noted that the large difference of total resorption volume was mainly due to the substantial volume increase in these two sectors in the heavy group.

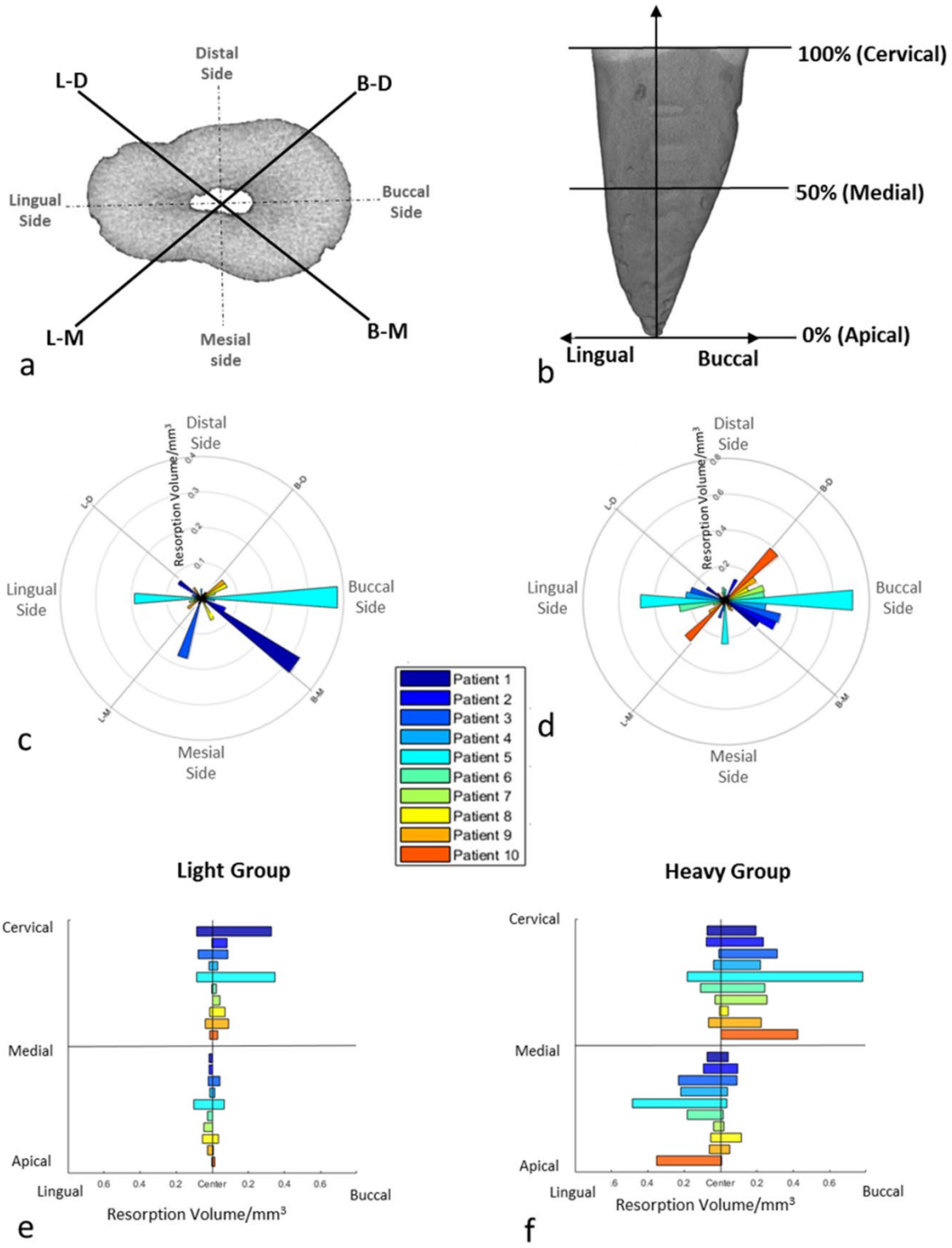

Figure 4. Spatial Location of Resorption Craters. a) Subdivisions for the assessment of the total resorption volume into four sectors: lingual, mesial, buccal and distal; b) Subdivisions for the assessment of the total resorption volume in upper-buccal, lower-buccal, upper-lingual and lower-lingual sectors along the root axis from apex; c) and d) Total resorption volume in individual patients in the sectors defined by a) for the light and heavy forces, respectively; e) and f) Total resorption volume in individual patients in the sectors defined by b) for the light and heavy forces, respectively.

3.4. Hydrostatic Pressure in Periodontal Ligament

Figures 5a and 5b show the spatial distribution of the hydrostatic pressure in the periodontal ligaments surrounding a pair of premolars under the two different loading conditions for one representative patient (Patient 10 as an example), with both buccal and lingual cross-sectional views. Deep blue (tensile) and dark red (compressive) indicate the affected areas where the hydrostatic stress exceeds the capillary blood pressure (4.7 kPa). The heavy group generally had larger affected areas than the light group did.

Similarly to Figures 4c-f, the sectional distribution of volume averaged hydrostatic stress ($\bar{\sigma}_H$) is summarised in Figures 5c-f for the two ways of subdividing the tooth into four sectors (see Figures 4a and 4b). In Figures 5c and 5d, the inward bars indicate the compressive hydrostatic stress and outward bars indicate the tensile hydrostatic stress. Both groups experienced much higher tensile and compressive stresses in the lingual and buccal sectors, as projected along the root. Under the heavier orthodontic load, tensile stress became dominant in the lingual sector, while compressive stress was dominant in the buccal sector (see Figure 5d).

Figures 5e and 5f focus on the buccal-lingual regions with the cervical and apical sectors being separated along the mid-plane of the roots (Figure 4b). The heavy orthodontic loading induced up to four-fold higher hydrostatic stress in the PDL than the light counterpart did. The apical-lingual and cervical-buccal sectors experienced compression, corresponding to the maximal resorption, while the other two sectors were in tension with minimal resorption observed.

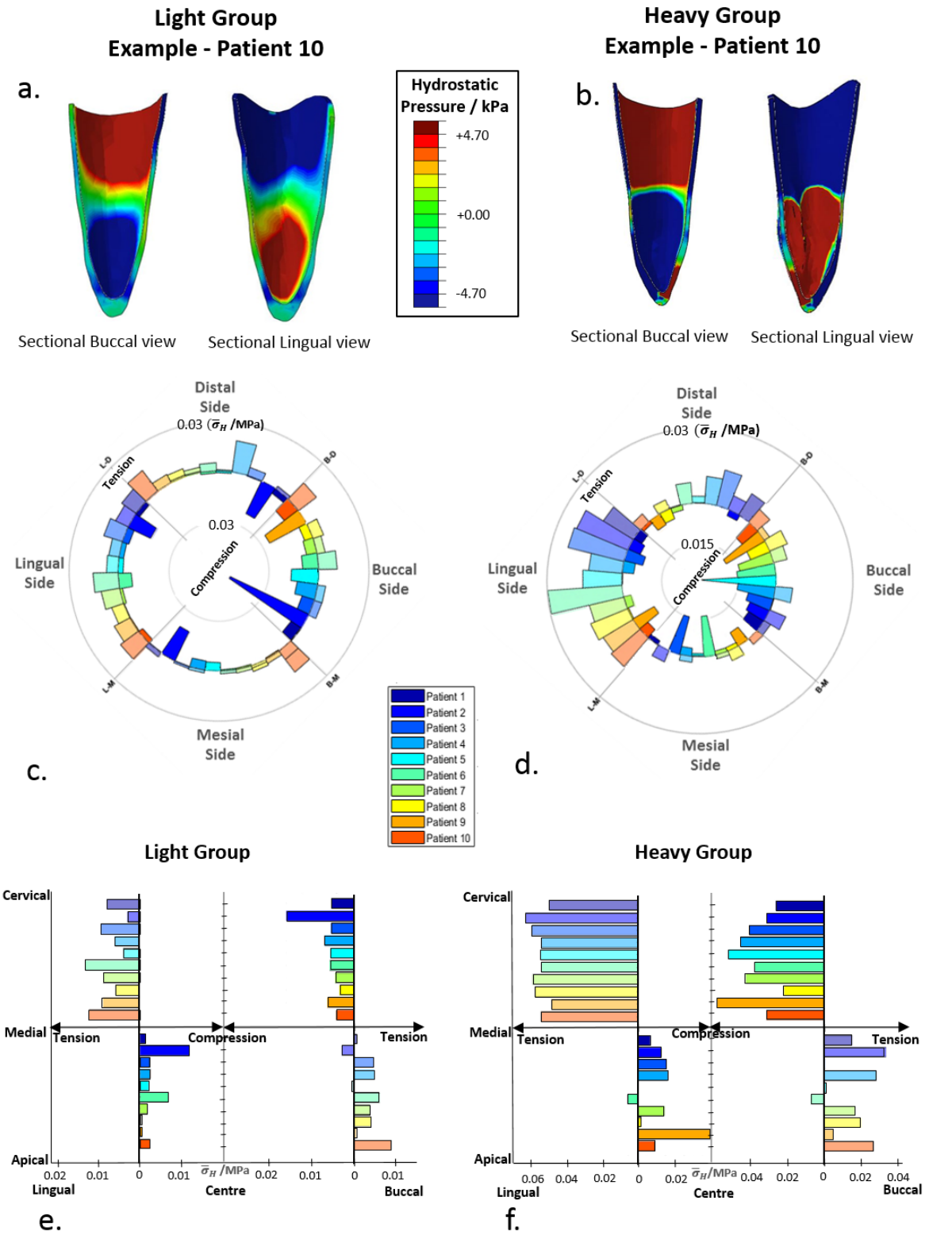

Figure 5. FEA Results of Hydrostatic Pressure in Periodontal Ligament. a) and b) the hydrostatic pressure distribution in corresponding PDLs with both buccal and lingual sectional views; c) and d) the sectional distribution of tensile (pointing outwards, translucent shaded) and compressive (pointing inwards, solid shaded) hydrostatic pressures in lingual, buccal, distal and mesial sectors as defined in Fig. 4a); e) and f) the sectional distribution of tensile (translucent shaded) and compressive (solid shaded) hydrostatic pressures in upper-buccal, upper-lingual, lower-buccal and lower lingual sectors as defined in Fig. 4b), under both light and heavy forces.

4. Discussion

4.1. Size and Shape Characteristics of Resorption Craters

Odontoclasts are a primary cell type responsible for ORR [18, 43]. In the early 1990s, Rygh et al. had observed that TRAP-positive odontoclasts crowded in the root resorption sites [17], suggesting that resorption craters resulted from the demineralisation activity of those multi-nucleated giant cells. Therefore, the patterns of resorption craters were interpreted as the result of *in-vivo* odontoclast activities induced by orthodontic forces, but we want to emphasize that this is a speculative interpretation since our study did not include any direct observations of cell activity. It should be noted that such a direct and timely-dependent observation of odontoclasts resorbing root and forming resorption pits in human patients is challenging (if not impossible) with the current experimental techniques available clinically.

Root resorption severity is quantified by the total resorption volume [29], which can be determined by the number of resorption craters and the individual crater size. Our results indicated that resorption severity was dependent on the magnitude of the applied orthodontic force. Compared with light forces, heavy forces led to greater total resorption volumes in all subjects. This rise of the total volume predominantly resulted from the increases in the volumes of individual craters, seen from the maximum and median crater sizes (Figures 2b and c). The large craters observed in the heavy group tended to have greater depth and larger surface dimension. In addition, we found a general tendency of greater crater numbers in the heavy group, but the significance of this increase ($\rho < 0.05$) was less than that of the individual size increase ($\rho < 0.001$).

With respect to the knowledge that odontoclasts were the main cell type that demineralises root surfaces [17, 18, 43], significant size increases of craters, such as those observed in this study, could

be a consequence of both enhancement of odontoclast resorption activity, and an increased number of odontoclasts acting in the same sites.

Although currently, no definitive characterisation of odontoclast responsive mechanisms to mechanical loading exists, one can, however, speculate about odontoclast behaviour from the relatively abundant studies on osteoclasts, attributable to the inherent similarities between these two cell types [18-20]. *In-vitro* investigations of stress-induced RANKL/RANK-mediated osteoclast behaviour are most relevant to the current study [19, 44, 45]. Osteoclast resorption activity commences after the 'seeding' of cells on mineral tissue surfaces by the formation of adhesion structures called sealing zones [21]. *In-vitro* studies have revealed that increasing mechanical stress not only directly enhances activated-osteoclast resorption ability [19], but also prolongs their life span [46, 47]. A combination of high mechanical stress and primary tissue breakdown may recruit more macrophages to resorption sites via mechano-biological signalling pathways, which are then subject to RANKL/RANK-mediated differentiation into new osteoclasts [19]. Based only on these characterisations of osteoclast behaviour, the authors suggest that similar mechanisms, primarily due to the improvements of odontoclast resorption ability and cellular recruitment, could be responsible for the observed increases in individual crater size. Conversely, correlations between osteoclast seeding, mechano-stimuli, and resorptive initiation have not been reported in the literature; and hence, cannot be used to explain the change in crater numbers. Clearly, while the imaging-based metrics used in this study provide certain evidence of cellular activity alone, odontoclast-specific *in-vitro* cell culture investigations are needed before draw more indicative conclusions divulging the relevant crater-formation mechanisms.

Further analysis of resorption crater shape revealed that the depth and surface aspect ratios

showed no significant differences between the different loading magnitudes (Figures 3a and 3b), suggesting an intrinsic proportional relationship between odontoclast resorption and progression ability. Majority of resorption trails was oriented at approximately 20 ± 10 degrees with respect to the root longitudinal axis in both heavy and light loading groups. While this correlation implies a preferential path for odontoclast progression, no direct evidence has been found in the literature to explain this particular orientation of progression for either odontoclasts or osteoclasts. Osteoclasts were reported to be sensitive to topographical discontinuities that were in the tens of microns in culture matrices [21-24], but there has yet been any clear evidence concerning the determinant factors for migration direction of such cells [24]. Possibly, odontoclast progression could be guided by micro/macro-morphological patterns on root surfaces, such as macroscopic surface curvature or surface asperities such as the micro-features resulted from PDL collagen fibre insertion and mineral crystal orientation [48], or the gradients of local mechanobiological stimulation. Nevertheless, this requires further investigation to reveal the underlying mechanisms dictating odontoclast progression.

4.2. Hydrostatic Pressure Distribution in PDL and Spatial Distribution of Craters

In this study, we calculated the volume averaged hydrostatic stress ($\bar{\sigma}_H$) in the PDL to quantify the initial mechanical stimulus for triggering root resorption. All PDLs were assumed to be 0.3 mm in thickness as reported in literature [11, 15, 31]. A sensitivity study on the PDL thickness was conducted in our *in-silico* models, showing that the differences of high tension/compression volume fraction (above 4.7 kPa) were within the standard deviation of ± 2.1% with virtually unchanged interstitial fluid pressure pattern in the PDL. Performing a spatial correlation between the locations where root resorption occurred and the distribution of $\bar{\sigma}_H$, we can provide three statements specifying the nature of the mechanical stimulus as follows.

First, the sign of the mechanical stimulus is important, with compressive stresses much more effectively triggering ORR than tensile stresses. To quantify how strongly resorption craters were concentrated in compressively stimulated regions (compression above 4.7kPa), we calculated the ratio between the percentage of resorption volume within the stimulated compressive/tensile region and the percentage of stimulated compressive/tensile volume out of the total volume of each PDL (*R-MS ratio*). Resorptions that occur randomly, i.e. independent from mechanical stimulus, would result in an *R-MS ratio* of 1. The resulting *R-MS ratios* were much greater for compressive stresses (light group: 1.96 and heavy group: 1.47) than for tensile stresses (light group: 0.70 and heavy group: 0.49). Therefore, the *in-silico* models showed that the compressed regions, which were in cervical-buccal and apical-lingual quarters due to the tipping nature of the orthodontic force, contained substantially more resorptions than in the tensile regions. Previous *in-vitro* studies have revealed that high compressive stresses lead to intense resorption activity; which is due to the increased localised tissue breakdown (debris) and cellular response in secreting RANKL/RANK, with enhanced macrophage recruitment and fusion to form odontoclasts [19, 45]. These biological responses to compressive loading are well-reflected by the dense spatial distribution of resorption craters observed in high compression zones, which also indicates the effectiveness of using $\bar{\sigma}_H$ as a measurement of mechano-stimulus for ORR when modelled *in-silico* as performed here. Moreover, our modelling results indicated that the increase of $\bar{\sigma}_H$ in tension was greater than that in compression when heavy loads were applied (Figure 5e and f). Nevertheless, we found no obvious changes of resorption severity in tensile regions (Figure 4e and f), suggesting that odontoclasts might not respond to the tensile mechano-stimulus evidently.

Second, not only is the sign of the stress important, but also the magnitude of stress is decisive

in triggering ORR. Considering compressive stresses in the interval between 2.35 and 4.7 kPa, the resulting *R-MS ratio* were 0.86 for light group and 0.72 for heavy, which is lower than 1 and substantially lower than the corresponding values of 1.96 and 1.47 when considering compressive stresses only above the threshold of capillary blood pressure (4.7kPa). Therefore, the present study provides evidence that compressive stress $\bar{\sigma}_H$ needs to exceed a threshold value comparable to the human capillary blood pressure to effectively initiate ORR.

Lastly, patient-specific factors, such as an individual's living habits, bone density and genetic factors, play an important multifactorial role in the mechanobiology for responsible for root resorption [2, 9, 49]. Although those patient-specific factors were inaccessible with the experimental design of this present study, we included the variation of individual's susceptibility to provide statistically comprehensiveness of the results. Following the rationale of this study by presenting the results for each patient individually, we calculated the *R-MS ratio* in high compressive regions for all the individuals and both teeth, the lightly and the heavily loaded. The results (see in Table 2) showed obvious variation among the patients, suggesting the individual variation in response to increased orthodontic forces. The larger values of the *R-MS ratio* for the light group in Table 2 are mainly due to a smaller region that is above the threshold value of compressive mechanical stimulation. A comparison between the values for the light and heavy loading in the same patient further shows no correlation. Both values particularly high (or low) would provide us with an indication that the mechano-regulation of ORR would have a high (or low) specificity in this patient. Rumpler et al. [50] revealed that osteoclast resorption ability, measured as the depth of resorption pits, was predominantly dependent on individual variation, and only marginally influenced by *in-vitro* culturing matrix material and surface roughness. This may also apply to odontoclasts since similar

variations in maximum crater size and depth between individuals were found in this study (e.g. Figure 2d, Figures 3a and 3b); and suggests a difference in the maximum resorption capability of odontoclasts in different individuals. Meanwhile, no clear relation between resorption volume and compressive $\bar{\sigma}_H$ in PDL were found (Figures 4 and 5), which also reflected individual variation in odontoclast sensitivity to changes in loading magnitude. Therefore, the authors believe that the mechano-stimulus in the PDL is one of the dominant factors of root resorption, but with substantial influence from other biological factors.

In addition, while ORR was reported to be positive proportional to OTM [51, 52], no clear correlation was found between the ORR severity and corresponding OTM distance of each tooth in the experiment presented here, which further demonstrated that an individual's response to orthodontic loading can be multifactorial.

Table 2. The *R-MS ratio* in high compressive regions for each subject

Patient ID	**1**	**2**	**3**	**4**	**5**	**6**	**7**	**8**	**9**	**10**
Light Group	2.31	1.44	1.87	1.77	2.47	2.64	2.64	2.03	2.58	0.95
Heavy Group	1.67	1.51	1.30	1.50	1.64	1.04	1.56	1.30	1.00	2.44

4.3. Limitation and Future Work

As with most numerical modelling studies on biological functional responses, the conclusions drawn from this work are subject to a series of assumptions. First, the TIVA approach tended to underestimate flat and shallow resorption craters, because deviations in the continuity of the surface boundary in these cases were often too marginal to be identified. Second, osteoclasts and odontoclasts have been assumed to behave physiologically in a similar way under mechanical loading. As a

consequence, a study on odontoclastic mechanisms without specific cellular models can only provide indirect evidence of *in-vivo* odontoclast activity. The present approach assumed that odontoclasts and osteoclasts have similar behaviour under mechano-stimulus because they are of the same cellular lineage and share the same mechanism of bio-molecule expression [18-20]. Additionally, the *ex-vivo* nature of the imaging analysis was considered to provide end-stage results for the *in-vivo* resorption phenomenon.

It should also be noted that the FE analysis in this study were based upon a population-generic anatomical model. Generic crowns and simplified jaws were adopted for the FE models, since there was a lack of accurate original anatomical information. However, such simplifications are widely accepted, and their effects on mechanical results have proved to be small [11, 31, 39].

To further understand the observations described in this paper and validate the resultant findings, odontoclast visualisation experiments should be conducted. Cryo-FIB/SEM can be utilised on animal models to reveal different stages of odontoclast behaviour during resorption development [53, 54], which will provide direct illustration of *in-vivo* circumstance. Potentially, a time-dependent multi-scale FEA can then be performed to better simulate the stress-induced cellular progress of root resorption, thereby creating an *in-silico* model describing odontoclastic activities with an improved patient-specific predictability of ORR in orthodontic treatment.

5. Conclusion

The work presented in this paper adopted a 3D microCT image analysis technique to characterise resorption craters on human root surfaces, which were further correlated to *in-silico* evaluations of mechano-stimulus. Within the given limitations, it was found that a certain level of compression in PDL predominantly augments individual crater size on root surface. A directional pattern of

resorption trails was found in both light and heavy groups. Based upon conventional interpretations of ORR, we speculate that these resorption trails reflect resorption and migration activities of odontoclasts, which requires more direct evidences with the advancement of experimental techniques to monitor *in-vivo* cellular behaviour at such an enclosed tissue interface.

Competing Interests

The authors declare no competing interests.

Data Accessibility

The datasets and codes supporting this article can be accessed via this link: https://cloudstor.aarnet.edu.au/plus/s/erocePG0H9mlfWM.

Authors' Contributions

J. Z carried out the Matlab scripting, statistical analyses, FE Modelling and data analysis, participated in the design of the study and drafted the manuscript; J. C participated in the design of the study and data analysis, and helped script Matlab codes and draft the manuscript; M.A.D collected clinical data; M.S, A.S and K.Z participated in data analysis and helped in draft the manuscript; R.W and Q.L conceived of the study, designed the study, coordinated the study and helped draft the manuscript. All authors gave final approval for publication.

Acknowledgement

This work was supported by Australian Research Council (ARC) through the Discovery (DP160104602) Scheme and Deutsche Forschungsgemeinschaft (DFG) through the Berlin-Brandenburg School for Regenerative Therapies GSC 203.

Table and Figure Caption List

Notes: Colour should be used for all figures in print.

Figure 1. Materials and Methods. a) An initial panoramic radiograph and lateral cephalogram were taken for each patient to ensure no abnormalities and resorption defects were present before treatment. b) Top view of orthodontic treatment setup including braces between the mandibular 1st molar and the 1st premolar and cement on top of the 1st molars (bluish). White arrows indicate buccally-directed orthodontic loads. Black arrows indicate the buccal and lingual directions, i.e. the outwards direction to the cheek and inwards direction to the tongue. c) schematic diagram of the Tomographic Interpolation and Volumetric Analysis (TIVA) procedure to determine resorption craters from a scanned root, through masking tooth root (cyan), edging (white), contour repair (white: original edge; red: repaired edge), re-masking (white), and mask subtraction (cyan: original tooth root mask; red: resorption craters mask). Black arrows indicate the orientation of the tooth with cervical defined towards the crown and apical towards the root apex. d) construction of a virtual assembly of the mandibular section by using virtually repaired root contour; e) meshed finite element model in commercial code ABAQUS with loading and boundary conditions.

Figure 2. Resorption Severity. a) Surface tomography of ten pairs of scanned 1st premolar roots, between heavy (225g) and light (25g) buccally directed orthodontic forces; b) Clinical records of Orthodontic Tooth Movement (OTM) among patients. c) total resorption volume and number of resorption craters for each patient; d) crater sizes in each patient. The Heavy group generally had larger craters than the Light group did. (The upper and lower box bands are the 1st and 3rd quartile, representing 25% to 75% of size observations. The bands inside boxes represent the median crater size for each subject. Craters with a size that exceeded 1.5 times that of the corresponding interquartile

range are plotted as outliers in this box-whisker chart.)

Figure 3. Crater Characteristics. a) and b) Correlation between resorption crater surface area and depth under light and heavy forces; c) and d) Correlation between crater orientation and surface aspect ratio, under light and heavy forces. Ax represents the surface long axis of craters whereas Bx represents the surface short axis. Z-axis is the longitudinal axis of the root.

Figure 4. Spatial Location of Resorption Craters. a) Subdivisions for the assessment of the total resorption volume into four sectors: lingual, mesial, buccal and distal; b) Subdivisions for the assessment of the total resorption volume in upper-buccal, lower-buccal, upper-lingual and lower-lingual sectors along the root axis from apex; c) and d) Total resorption volume in individual patients in the sectors defined by a) for the light and heavy forces, respectively; e) and f) Total resorption volume in individual patients in the sectors defined by b) for the light and heavy forces, respectively.

Figure 5. FEA Results of Hydrostatic Pressure in Periodontal Ligament. a) and b) the hydrostatic pressure distribution in corresponding PDLs with both buccal and lingual sectional views; c) and d) the sectional distribution of tensile (pointing outwards, translucent shaded) and compressive (pointing inwards, solid shaded) hydrostatic pressures in lingual, buccal, distal and mesial sectors as defined in Fig. 4a); e) and f) the sectional distribution of tensile (translucent shaded) and compressive (solid shaded) hydrostatic pressures in upper-buccal, upper-lingual, lower-buccal and lower lingual sectors as defined in Fig. 4b), under both light and heavy forces.

Table 1. Material properties adopted in tooth movement simulation.

Material	Young's Modulus (MPa)	Poisson's Ratio
Root (Dentin)	18,600	0.31
Cortical bone	14,700	0.31
Trabecular bone	490	0.3
PDL	Hyperelastic (Ogden 4th)	0.45

Table 2. The *R-MS ratio* in high compressive regions for each subjects.

Patient ID	**1**	**2**	**3**	**4**	**5**	**6**	**7**	**8**	**9**	**10**
Light Group	2.31	1.44	1.87	1.77	2.47	2.64	2.64	2.03	2.58	0.95
Heavy Group	1.67	1.51	1.30	1.50	1.64	1.04	1.56	1.30	1.00	2.44

References

[1] Uhde, M.D., Sadowsky, C. & BeGole, E.A. 1983 Long-term stability of dental relationships after orthodontic treatment. *Angle Orthod* **53**, 240-252. (doi:10.1043/0003-3219(1983)053<0240:LSODRA>2.0.CO;2).

[2] Newman, W.G. 1975 Possible etiologic factors in external root resorption. *Am. J. Orthod. Dentofac. Orthop.* **67**, 522-539. (doi:10.1016/0002-9416(75)90298-5).

[3] Brezniak, N. & Wasserstein, A. 1993 Root resorption after orthodontic treatment: Part 1. Literature review. *American Journal of Orthodontics and Dentofacial Orthopedics* **103**, 62-66. (doi:10.1016/0889-5406(93)70106-X).

[4] Roscoe, M.G., Meira, J.B. & Cattaneo, P.M. 2015 Association of orthodontic force system and root resorption: A systematic review. *Am J Orthod Dentofacial Orthop* **147**, 610-626. (doi:10.1016/j.ajodo.2014.12.026).

[5] von Bohl, M. & Kuijpers-Jagtman, A.M. 2009 Hyalinization during orthodontic tooth movement: a systematic review on tissue reactions. *Eur J Orthod* **31**, 30-36. (doi:10.1093/ejo/cjn080).

[6] Lunardi, D., Bécavin, T., Gambiez, A. & Deveaux, É. 2013 Orthodontically induced inflammatory root resorption: apical and cervical complications. *Journal of Dentofacial Anomalies and Orthodontics* **16**. (doi:10.1051/odfen/2012402).

[7] Patel, S., Ricucci, D., Durak, C. & Tay, F. 2010 Internal root resorption: a review. *J Endod* **36**, 1107-1121. (doi:10.1016/j.joen.2010.03.014).

[8] Fernandes, M., de Ataide, I. & Wagle, R. 2013 Tooth resorption part I - pathogenesis and case series of internal resorption. *J Conserv Dent* **16**, 4-8. (doi:10.4103/0972-0707.105290).

[9] Sameshima, G.T. & Sinclair, P.M. 2001 Predicting and preventing root resorption: Part I. Diagnostic factors. *Am J Orthod Dentofacial Orthop* **119**, 505-510. (doi:10.1067/mod.2001.113409).

[10] Naveh, G.R.S., Brumfeld, V., Shahar, R. & Weiner, S. 2013 Tooth periodontal ligament: Direct 3D microCT visualization of the collagen network and how the network changes when the tooth is loaded. *Journal of Structural Biology* **181**, 108-115. (doi:10.1016/j.jsb.2012.10.008).

[11] Chen, J., Li, W., Swain, M.V., Ali Darendeliler, M. & Li, Q. 2014 A periodontal ligament driven remodeling algorithm for orthodontic tooth movement. *J Biomech* **47**, 1689-1695. (doi:10.1016/j.jbiomech.2014.02.030).

[12] Field, C., Ichim, I., Swain, M.V., Chan, E., Darendeliler, M.A., Li, W. & Li, Q. 2009 Mechanical responses to orthodontic loading: a 3-dimensional finite element multi-tooth model. *Am J Orthod Dentofacial Orthop* **135**, 174-181. (doi:10.1016/j.ajodo.2007.03.032).

[13] Hohmann, A., Wolfram, U., Geiger, M., Boryor, A., Kober, C., Sander, C. & Sander, F.G. 2009 Correspondences of hydrostatic pressure in periodontal ligament with regions of root resorption: a clinical and a finite element study of the same human teeth. *Comput Methods Programs Biomed* **93**, 155-161. (doi:10.1016/j.cmpb.2008.09.004).

[14] Rygh, P. 1977 Orthodontic root resorption studied by electron microscopy. *Angle Orthod* **47**, 1-16. (doi:10.1043/0003-3219(1977)047<0001:ORRSBE>2.0.CO;2).

[15] Berkovitz, B.K., Holland, G.R. & Moxham, B.J. 2016 *Oral anatomy, histology and embryology*, Elsevier.

[16] Mavragani, M., Amundsen, O.C., Selliseth, N.J., Brudvik, P. & Selvig, K.A. 2004 Early root alterations after orthodontic force application studied by light and scanning electron microscopy. *Eur J Orthod* **26**, 119-128. (doi:10.1093/ejo/26.2.119).

[17] Brudvik, P. & Rygh, P. 1994 Root resorption beneath the main hyalinized zone. *The European Journal of Orthodontics* **16**, 249-263. (doi:10.1093/ejo/16.4.249).
[18] Sasaki, T. 2003 Differentiation and functions of osteoclasts and odontoclasts in mineralized tissue resorption. *Microsc Res Tech* **61**, 483-495. (doi:10.1002/jemt.10370).
[19] Kamat, M., Puranik, R., Vanaki, S. & Kamat, S. 2013 An insight into the regulatory mechanisms of cells involved in resorption of dental hard tissues. *Journal of oral and maxillofacial pathology: JOMFP* **17**, 228-233. (doi:10.4103/0973-029X.119736).
[20] Hammarstrom, L. & Lindskog, S. 1985 General morphological aspects of resorption of teeth and alveolar bone. *Int Endod J* **18**, 93-108. (doi: 10.1111/j.1365-2591.1985.tb00426.x).
[21] Geblinger, D., Geiger, B. & Addadi, L. 2009 Surface-induced regulation of podosome organization and dynamics in cultured osteoclasts. *Chembiochem* **10**, 158-165. (doi:10.1002/cbic.200800549).
[22] Shemesh, M., Addadi, S., Milstein, Y., Geiger, B. & Addadi, L. 2016 Study of Osteoclast Adhesion to Cortical Bone Surfaces: A Correlative Microscopy Approach for Concomitant Imaging of Cellular Dynamics and Surface Modifications. *ACS Appl Mater Interfaces* **8**, 14932-14943. (doi:10.1021/acsami.5b08126).
[23] Luxenburg, C., Geblinger, D., Klein, E., Anderson, K., Hanein, D., Geiger, B. & Addadi, L. 2007 The architecture of the adhesive apparatus of cultured osteoclasts: from podosome formation to sealing zone assembly. *PLoS One* **2**, e179. (doi:10.1371/journal.pone.0000179).
[24] Rumpler, M., Wurger, T., Roschger, P., Zwettler, E., Peterlik, H., Fratzl, P. & Klaushofer, K. 2012 Microcracks and osteoclast resorption activity in vitro. *Calcif Tissue Int* **90**, 230-238. (doi:10.1007/s00223-011-9568-z).
[25] Bosshardt, D.D., Stadlinger, B. & Terheyden, H. 2015 Cell-to-cell communication–periodontal regeneration. *Clinical oral implants research* **26**, 229-239. (doi:10.1111/clr.12543).
[26] Kitaura, H., Fujimura, Y., Yoshimatsu, M., Eguchi, T., Kohara, H., Jang, I., Morita, Y. & Yoshida, N. 2009 An M-CSF Receptor c-Fms Antibody Inhibits Mechanical Stress–Induced Root Resorption during Orthodontic Tooth Movement in Mice. *The Angle Orthodontist* **79**, 835-841. (doi:10.2319/080708-412.1).
[27] Paetyangkul, A., Turk, T., Elekdag-Turk, S., Jones, A.S., Petocz, P. & Darendeliler, M.A. 2009 Physical properties of root cementum: part 14. The amount of root resorption after force application for 12 weeks on maxillary and mandibular premolars: a microcomputed-tomography study. *Am J Orthod Dentofacial Orthop* **136**, 492 e491-499; discussion 492-493. (doi:10.1016/j.ajodo.2009.03.008).
[28] King, G.J. & Fischlschweiger, W. 1982 The effect of force magnitude on extractable bone resorptive activity and cemental cratering in orthodontic tooth movement. *J Dent Res* **61**, 775-779. (doi:10.1177/00220345820610062501).
[29] Chan, E.K., Darendeliler, M.A., Petocz, P. & Jones, A.S. 2004 A new method for volumetric measurement of orthodontically induced root resorption craters. *Eur J Oral Sci* **112**, 134-139. (doi:10.1111/j.1600-0722.2004.00118.x).
[30] Murphy, C., Kalajzic, Z., Chandhoke, T., Utreja, A., Nanda, R. & Uribe, F. 2016 The effect of corticision on root resorption with heavy and light forces. *Angle Orthod* **86**, 17-23. (doi:10.2319/112514-843.1).
[31] Liao, Z.P., Chen, J.N., Li, W., Darendeliler, M.A., Swain, M. & Li, Q. 2016 Biomechanical investigation into the role of the periodontal ligament in optimising orthodontic force: a finite element

case study. *Archives of Oral Biology* **66**, 98-107. (doi:10.1016/j.archoralbio.2016.02.012).
[32] Chan, E. & Darendeliler, M.A. 2005 Physical properties of root cementum: Part 5. Volumetric analysis of root resorption craters after application of light and heavy orthodontic forces. *Am J Orthod Dentofacial Orthop* **127**, 186-195. (doi:10.1016/j.ajodo.2003.11.026).
[33] Hazel, R., Rohan, G. & West, V. 1984 Force relaxation in orthodontic arch wires. *American journal of orthodontics* **86**, 396-402. (doi:10.1016/S0002-9416(84)90032-0).
[34] Cattaneo, P.M., Dalstra, M. & Melsen, B. 2005 The finite element method: a tool to study orthodontic tooth movement. *Journal of Dental Research* **84**, 428-433. (doi:10.1177/154405910508400506).
[35] Chen, J., Ahmad, R., Li, W., Swain, M. & Li, Q. 2015 Biomechanics of oral mucosa. *J R Soc Interface* **12**, 20150325. (doi:10.1098/rsif.2015.0325).
[36] Huang, H., Tang, W., Yan, B., Wu, B. & Cao, D. 2016 Mechanical responses of the periodontal ligament based on an exponential hyperelastic model: a combined experimental and finite element method. *Comput Methods Biomech Biomed Engin* **19**, 188-198. (doi:10.1080/10255842.2015.1006207).
[37] Toms, S.R., Lemons, J.E., Bartolucci, A.A. & Eberhardt, A.W. 2002 Nonlinear stress-strain behavior of periodontal ligament under orthodontic loading. *American Journal of Orthodontics and Dentofacial Orthopedics* **122**, 174-179. (doi:10.1067/mod.2002.124997).
[38] Pietrzak, G., Curnier, A., Botsis, J., Scherrer, S., Wiskott, A. & Belser, U. 2002 A nonlinear elastic model of the periodontal ligament and its numerical calibration for the study of tooth mobility. *Computer methods in biomechanics and biomedical engineering* **5**, 91-100. (doi:10.1080/10255840290032117).
[39] Liao, Z., Chen, J., Zhang, Z., Li, W., Swain, M. & Li, Q. 2015 Computational modeling of dynamic behaviors of human teeth. *J Biomech* **48**, 4214-4220. (doi:10.1016/j.jbiomech.2015.10.019).
[40] Zhang, Z., Chen, J., Li, E., Li, W., Swain, M. & Li, Q. 2016 Topological design of all-ceramic dental bridges for enhancing fracture resistance. *Int J Numer Method Biomed Eng* **32**. (doi:10.1002/cnm.2749).
[41] Chen, J.N., Ahmad, R., Suenaga, H., Li, W., Swain, M. & Li, Q. 2015 A comparative study on complete and implant retained denture treatments - A biomechanics perspective. *Journal of Biomechanics* **48**, 512-519. (doi:10.1016/j.jbiomech.2014.11.043).
[42] Field, C., Li, Q., Li, W., Thompson, M. & Swain, M.J.J.o.b. 2010 Prediction of mandibular bone remodelling induced by fixed partial dentures. **43**, 1771-1779. (doi: 10.1016/j.jbiomech.2010.02.016).
[43] Iglesias-Linares, A. & Hartsfield, J.K., Jr. 2017 Cellular and Molecular Pathways Leading to External Root Resorption. *J Dent Res* **96**, 145-152. (doi:10.1177/0022034516677539).
[44] Heinrich, J., Bsoul, S., Barnes, J., Woodruff, K. & Abboud, S. 2005 CSF-1, RANKL and OPG regulate osteoclastogenesis during murine tooth eruption. *Arch Oral Biol* **50**, 897-908. (doi:10.1016/j.archoralbio.2005.02.007).
[45] Kanzaki, H., Chiba, M., Shimizu, Y. & Mitani, H. 2002 Periodontal Ligament Cells Under Mechanical Stress Induce Osteoclastogenesis by Receptor Activator of Nuclear Factor κB Ligand Up-Regulation via Prostaglandin E2 Synthesis. *Journal of Bone and Mineral Research* **17**, 210-220. (doi:10.1359/jbmr.2002.17.2.210).
[46] Fuller, K., Wong, B., Fox, S., Choi, Y.W. & Chambers, T.J. 1998 TRANCE is necessary and sufficient for osteoblast-mediated activation of bone resorption in osteoclasts. *Journal of*

Experimental Medicine **188**, 997-1001. (doi:DOI 10.1084/jem.188.5.997).
[47] Weinstein, R.S., Chen, J.R., Powers, C.C., Stewart, S.A., Landes, R.D., Bellido, T., Jilka, R.L., Parfitt, A.M. & Manolagas, S.C. 2002 Promotion of osteoclast survival and antagonism of bisphosphonate-induced osteoclast apoptosis by glucocorticoids. *J Clin Invest* **109**, 1041-1048. (doi:10.1172/JCI14538).
[48] Marten, A., Fratzl, P., Paris, O. & Zaslansky, P. 2010 On the mineral in collagen of human crown dentine. *Biomaterials* **31**, 5479-5490. (doi:10.1016/j.biomaterials.2010.03.030).
[49] Brezniak, N. & Wasserstein, A. 1993 Root resorption after orthodontic treatment: Part 2. Literature review. *American Journal of Orthodontics and Dentofacial Orthopedics* **103**, 138-146. (doi: 10.1016/S0889-5406(05)81763-9).
[50] Rumpler, M., Wurger, T., Roschger, P., Zwettler, E., Sturmlechner, I., Altmann, P., Fratzl, P., Rogers, M.J. & Klaushofer, K. 2013 Osteoclasts on bone and dentin in vitro: mechanism of trail formation and comparison of resorption behavior. *Calcif Tissue Int* **93**, 526-539. (doi:10.1007/s00223-013-9786-7).
[51] Parker, R.J. & Harris, E.F. 1998 Directions of orthodontic tooth movements associated with external apical root resorption of the maxillary central incisor. *American journal of orthodontics and dentofacial orthopedics* **114**, 677-683. (doi:10.1016/S0889-5406(98)70200-8).
[52] Weltman, B., Vig, K.W., Fields, H.W., Shanker, S. & Kaizar, E.E. 2010 Root resorption associated with orthodontic tooth movement: a systematic review. *American Journal of Orthodontics and Dentofacial Orthopedics* **137**, 462-476. (doi:10.1016/j.ajodo.2009.06.021).
[53] Kizilyaprak, C., Bittermann, A.G., Daraspe, J. & Humbel, B.M. 2014 FIB-SEM tomography in biology. In *Electron Microscopy: Methods and Protocols, 3rd Edition* (ed. J. Kuo), pp. 541-558.
[54] Kerschnitzki, M., Akiva, A., Ben Shoham, A., Asscher, Y., Wagermaier, W., Fratzl, P., Addadi, L. & Weiner, S. 2016 Bone mineralization pathways during the rapid growth of embryonic chicken long bones. *J Struct Biol* **195**, 82-92. (doi:10.1016/j.jsb.2016.04.011).